IET Power Electronics

The Institution of Engineering and Technology WILEY

ORIGINAL RESEARCH PAPER
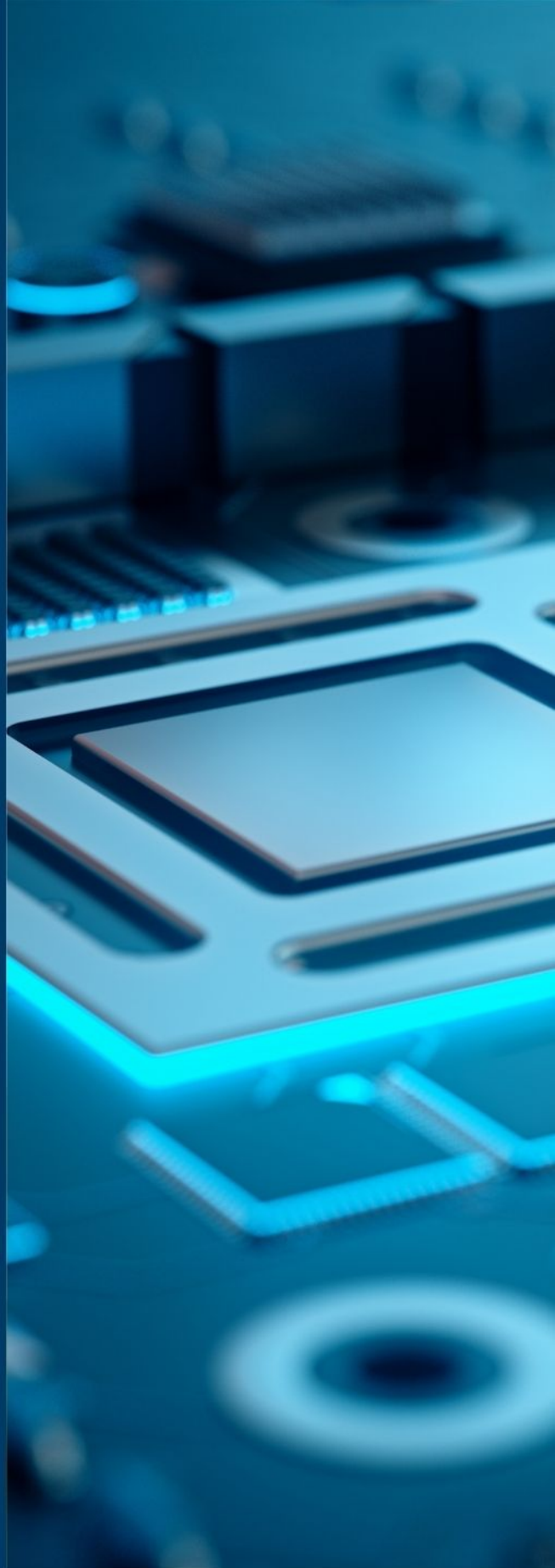
Investigation of a bidirectional DC/DC converter with zero-voltage switching operation for battery interfaces

Veera Venkata Subrahmanya Kumar Bhajana[1] | **Pavel Drabek**[2] | **Martin Jara**[2] | **Madhuchandra Popuri**[3] | **Atif Iqbal**[4] | **Chitti Babu B.**[5]

[1] School of Electronics Engineering, KIIT University, Bhubaneswar, Orissa, India

[2] Department of Electromechanics and Power Electronics, Regional Innovation Centre for Electrical Engineering, University of West Bohemia, Pilsen, Czech Republic

[3] School of Electrical Engineering, KIIT University, Bhubaneswar, Orissa, India

[4] Department of Electrical Engineering, Qatar University, Doha, Qatar

[5] Department of Electronics Engineering, Indian Institute of Information Technology, Design and Manufacturing, Kancheepuram, Chennai, Tamil Nadu, India

Correspondence

Veera Venkata Subrahmanya Kumar Bhajana, Campus-12 School of Electronics Engineering, KIIT University, Bhubaneswar 751024, Orissa, India.
Email: bvvs.kumarfet@kiit.ac.in

Abstract

This paper proposes a bidirectional DC–DC converter with soft-switching capabilities. The main characteristic of this converter is that it can be operated in both boost and buck modes. The major advantages of this converter are high efficiency and reduced switching loss in high-power and high-voltage applications. The soft-switching capability is obtained by additional dual auxiliary resonant circuits connected to the conventional non-isolated bidirectional DC–DC converter. Except for the auxiliary switches, all main switches turn on with zero-voltage switching in this proposed bidirectional DC–DC converter. The auxiliary switches turn off with zero current transition. The principle of operation, theoretical analysis and experimental results of a 175 V/385 V bidirectional DC–DC converter at 2 kW output power with switching frequency of 50 kHz are provided. The experimental results verified the zero-voltage switching operation for boost and buck modes with efficiencies 96.5% and 96%, respectively, at full load.

1 | INTRODUCTION

Isolated and non-isolated DC–DC converters are playing an important role in battery-charging applications. Different types of non-isolated converters, such as boost [1], buck [2] and buck–boost [3, 4], are widely used to obtain desired voltages, which depend on the ability of the fuel cells, super-capacitors and photo-voltaic cells. To recapture a large burst of power and capture braking energy, an actively controlled hybrid magnetic battery/ultra-capacitor based energy storage system was proposed [5], which effectively improves the lifetime of batteries without considerable voltage stresses. As against conventional buck–boost DC–DC converter [6], coupled inductor based bidirectional converters (BDC) [7–9] are the alternate solutions to enlarge voltage gain with low circulating current and lower conduction losses. However, voltage stress in switching devices may increase due to the additional coupled induc-

tor. On the other hand an interleaved boost converter structure [10] with an additional coupled inductor and active clamp circuits has been investigated to obtain high-voltage conversion ratio with soft switching. Recent work on BDC [11] with a coupled inductor demonstrates the significant benefits such as high-power density and high conversion ratios. On the other hand, a magnetic coupling structure with additional auxiliary switches is utilised in BDC [12] to have soft-switching turn on, that is, zero-voltage switching (ZVS). In spite of these advantages, the coupling structure may have additional core losses. In another literature soft switching is achieved in a BDC [13] with the help of diodes, snubber capacitors and coupled inductors as a part of auxiliary circuit in addition to the conventional buck–boost structure. Also, to mitigate the drawbacks in the earlier converters, an energy recycling technique [14] is used through active clamp circuits combined with two cascaded boost converters. Similarly, an active clamp circuit based BDC [15] and interleaved

step-up/step-down DC–DC converter [16] have ZVS turn on, thereby achieving high efficiency at light loads. On the other hand, adopting an inductor and capacitors in a conventional BDC [17], makes the structure simpler and ripple free inductor current is obtained. Nevertheless, this converter is preferred for low voltage low power applications. In order to limit the circulating current and to achieve ZVS operation over a wide range of loads, a BDC [18] is added with auxiliary switches, an inductor and diodes. A high-gain BDC [19] provides ZVS for wide-range duty cycle and high-power levels, which utilises dual auxiliary resonant networks. A soft-switched non-isolated BDC [20] is also developed with an additional auxiliary circuit, which includes a coupled inductor and auxiliary switches. This converter is smaller in size as all the magnetic components are on a single core and also minimises turn-on switching losses. However, it can be used for high-voltage low-power converter systems.

The main attention of this paper is to propose a new ZVS non-isolated BDC with dual auxiliary resonant circuit for high-voltage high-power applications. The ZVS turn-on can be obtained in the main switches regardless of direction of power transfer. This converter has utmost benefits, firstly, the turn-on of main switches with ZVS and secondly, auxiliary switches are turned off with zero current transition (ZCT). The proposed converter is tested on 175 V/385 V converter system, which is operated at 50 kHz switching frequency and efficiency measured up to a maximum output power of 2 kW. Furthermore, the performance of this converter is analysed at different duty ratios in both boost and buck modes. The principle of operation is presented in Section 2, while the design and simulation analysis are illustrated in Sections 3 and 4, respectively. Experimental investigations are exhibited in Section 5.

2 | GENERAL CONFIGURATION OF PROPOSED CONVERTER AND OPERATIONAL PRINCIPLES

The general configuration of proposed non-isolated ZVS BDC is shown in Figure 1. The main power transfer switches S_1, S_2 and the auxiliary resonant network comprises two auxiliary switches, S_s, S_p, two resonant inductors, L_s, L_p and two resonant capacitors, C_s, C_p. The main switch, S_2 is turned on with ZVS by turning on auxiliary switch, S_s for a short duration, when the converter is operated in boost mode. Similarly, while the converter is operated in buck mode, the ZVS turn-on of S_1 can be obtained through the auxiliary switch S_p. In both boost and buck operations, the auxiliary switches (S_s, S_p) are turned on for a short period before the main switches (S_1, S_2) get commutated from the turning off state. The auxiliary switches S_s, S_p are turned off through ZCT. In this proposed converter, all semiconductor devices are soft-switched in both modes of operations. The equivalent schematics of boost and buck modes are shown in Figure 2(a) and (b). The principle of operation of the converter is divided into eight time intervals for boost and buck modes. The operating principles are described with the help of key waveform shown in Figure 3 and current flow equiva-
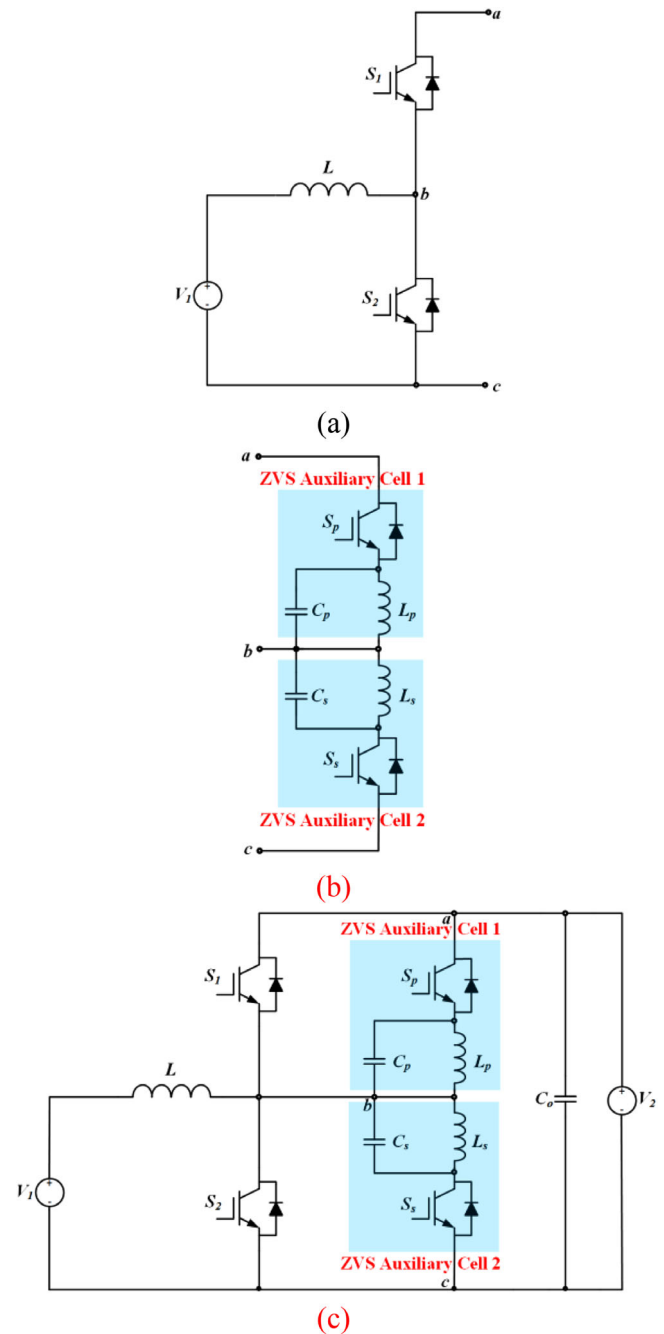

FIGURE 1 Derivation of ZVS bidirectional converter: (a) conventional bidirectional cell, (b) dual auxiliary ZVS cell and (c) proposed bidirectional converter

lent schematics of each interval are shown in Figures 4(a)–(d) and 5(a)–(d), respectively.

2.1 | Boost mode

The boost mode operation is divided into eight intervals from t_0 to t_8. Figure 3 shows the steady-state waveforms of V_{S2} and currents i_{S2}, i_{Ss}, inductor current, i_{Ls} and voltages across capacitor, C_s as V_{Cs}. All these waveforms are with respect to the gate pulses of V_{g2}, V_{gs} and the equivalent current flow
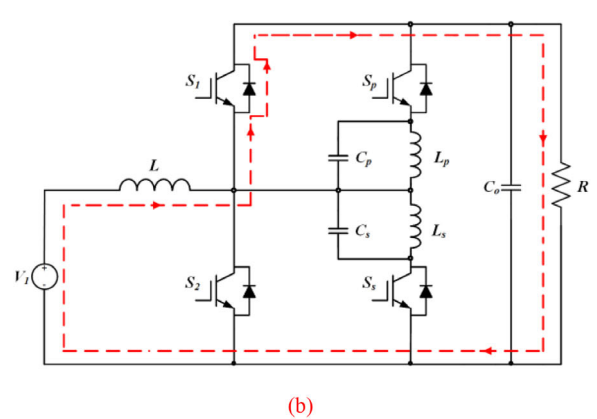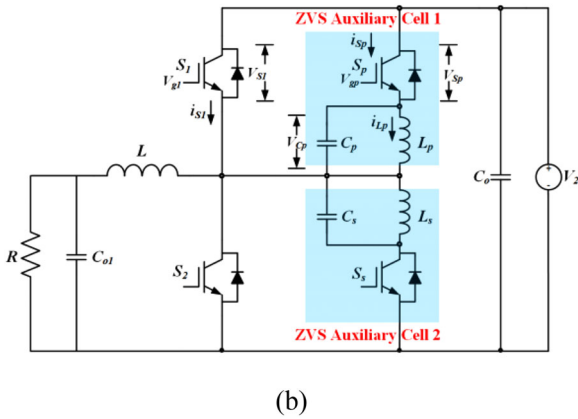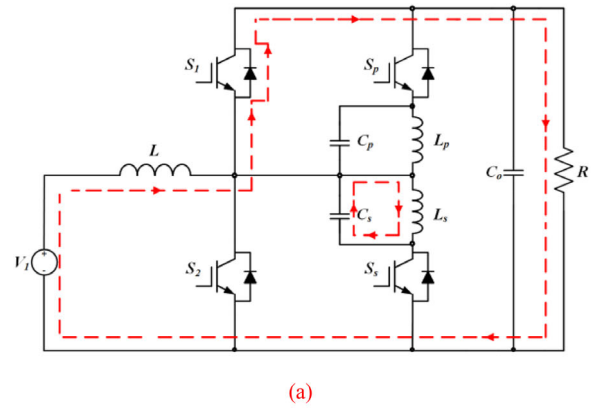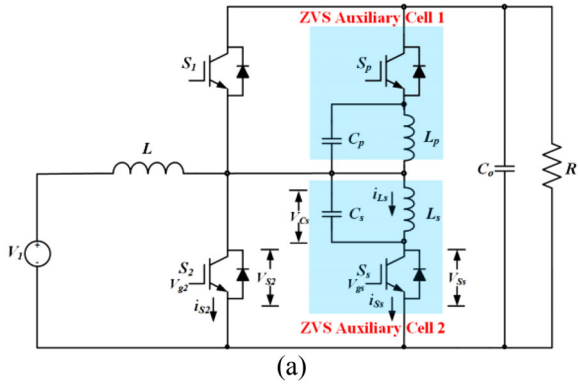
FIGURE 2   Equivalent circuits: (a) boost mode and (b) buck mode
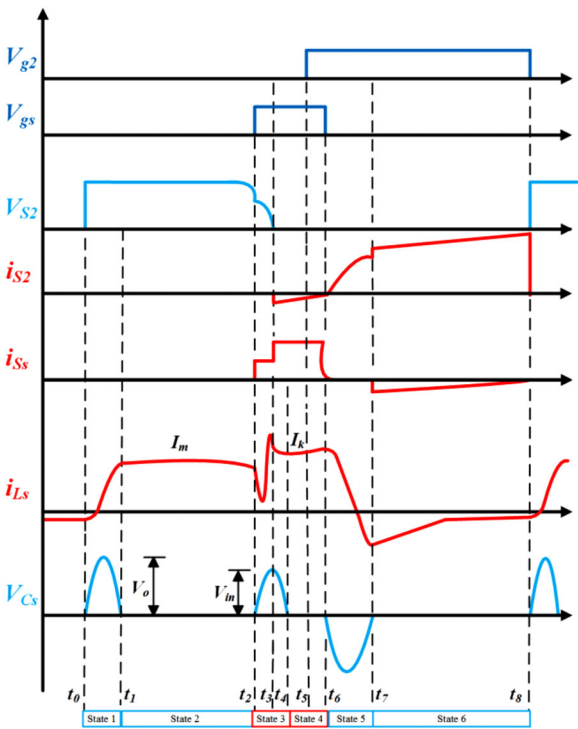
FIGURE 3   Steady-state waveforms: boost mode (V_{g1}: gate voltage S_2; V_{gs}: gate voltage S_s; V_{S2}: collector–emitter voltage S_2; i_{S2}: current through S_2; i_{Ss}: current through S_s; i_{Ls}: resonant inductor L_s current; V_{Cs}: voltage across resonant capacitor C_s
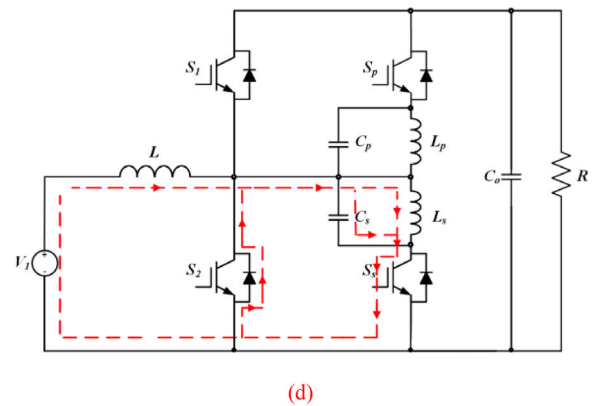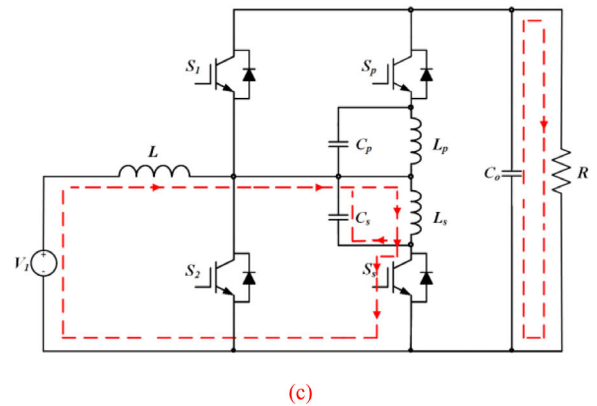
FIGURE 4   Equivalent current flow schematics : boost mode (a) interval (t_0–t_1), (b) interval (t_1–t_2), (c) interval (t_2–t_3) and (d) interval (t_3–t_4)
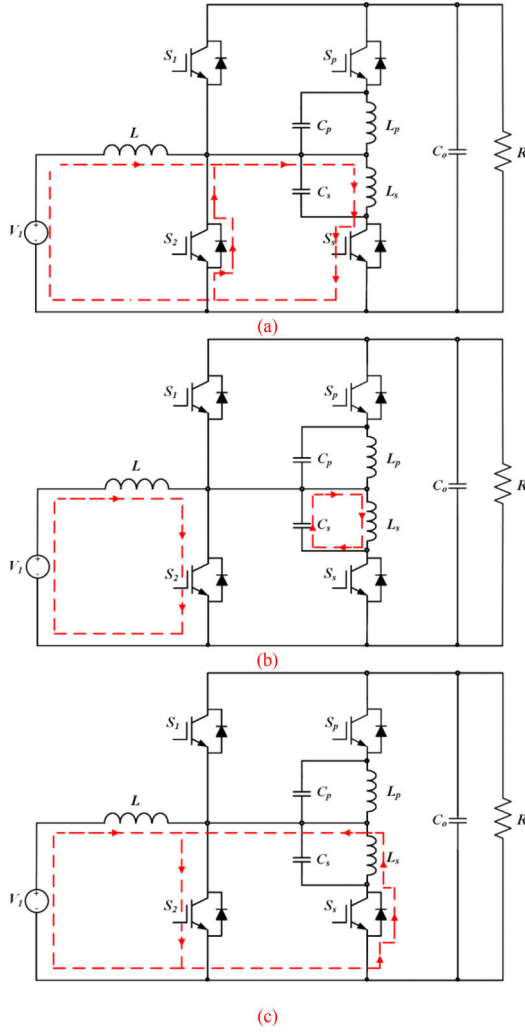
FIGURE 5 Equivalent current flow schematics: boost mode (a) interval (t_4-t_5), (b) interval (t_5-t_6) and (c) intervals (t_6-t_7) and (t_7-t_8)

schematics for all eight intervals (t_0 to t_8) for the boost mode are shown in Figures 4(a)–(d) and 5(a)–(c). The eight intervals further classified into six different states of which three are resonant (states 1, 3 and 5) and rest are non-resonant (states 2, 4 and 6). The intervals are considered as follows: t_0– t_1 is state 1; t_1–t_2 is state 2; t_2–t_3 and t_3–t_4 are state 3; t_4–t_5 and t_5–t_6 are state 4; t_6–t_7 is state 5 and t_7–t_8 is state 6. All the eight intervals are described as follows:

Interval (t_0-t_1): This interval starts when switches S_2, S_s are turned off at the same time. During this stage, the power is delivered to load via accumulated energy by L through the body diode of S_1. The voltage across C_s is charged to the level of output voltage after half cycle and V_{Cs} is completely discharged at t_1. L_s current, i_{Ls} linearly increases and at t_1, i_{Ls} reaches a constant, I_m. The i_{Ls} and V_{Cs} are expressed as follows:

$$i_{Ls}(t) = i_{Ls}(t_0) \cos \omega(t - t_0) \tag{1}$$

$$V_{Cs}(t) = Z \sin \omega(t - t_0) \tag{2}$$

$$V_{Cs}(t) = \frac{\alpha I_{in}}{V_o} \sin \omega(t - t_0) \tag{3}$$

$$\Delta t_0 = \frac{1}{\sqrt{L_s C_s}} \cos^{-1} \left(\frac{I_m}{i_{Ls}(t_0)} \right). \tag{4}$$

Interval (t_1-t_2): During this interval, the power is delivered to load via the input inductor L and body diode of S_1:

$$V_L = V_1 - V_o \tag{5}$$

$$i_{Ls} = I_m \tag{6}$$

$$V_{Cs} = 0. \tag{7}$$

Interval (t_2--t_3): This interval begins with the turn on of auxiliary IGBT, S_s to obtain ZVS turn on of S_2. In this short interval, the capacitor C_s begins to charge to the input voltage level, V_1 and inductor current will increase linearly. When voltage across C_s reaches the input voltage, V_{S2} smoothly reduces to zero and L_s current increases to peak current, I_k which is equal to I_o. V_L, V_{Cs}, i_{Ls} and the time interval equations are expressed as

$$V_L = V_1 - V_{Ls} \tag{8}$$

$$i_{Ls}(t) = i_{Ls}(t_2) \cos \omega(t - t_2) \tag{9}$$

$$V_{Cs}(t) = Z \sin \omega(t - t_2) \tag{10}$$

$$i_{Ls}(t_2) = I_k \tag{11}$$

$$I_k = i_{Ls}(t_3) \cos \omega(t_3 - t_2) \tag{12}$$

$$\Delta t_2 = \frac{1}{\omega} \cos^{-1} \left(\frac{I_k}{i_{Ls}(t_2)} \right) \tag{13}$$

$$V_{Cs}(t) = \frac{\alpha I_{in}}{V_o} \sin \omega(t - t_2) \tag{14}$$

$$\alpha = \sqrt{\frac{Ls}{Cs}} \times \frac{V_o}{I_{in}}, \tag{15}$$

where $\omega = \frac{1}{\sqrt{L_s C_s}}$; $Z = \sqrt{\frac{L_s}{C_s}}$.

Interval (t_3-t_4): At the beginning of this interval, the body diode of S_2 starts conducting to allow the resonant current. There is still a resonance between L_s and C_s and the capacitor, C_s starts discharging and gets completely discharged at t_4.

Interval (t_4-t_5): At the beginning of this interval, the capacitor C_s is completely discharged. The auxiliary IGBT S_s is in conducting state and body diode of S_2 will continue to conduct.

Interval (t_5-t_6): At t_5, the gate pulse, V_{g2} is applied to S_2. Since S_2 has zero voltage at the instant of turn on, ZVS turn on is achieved. At t_5, the body diode of S_2 is turned off and current through the S_s smoothly reduces to zero, such that the ZCS turn-off operation is achieved. The equations for L_s current and voltage across C_s are as follows:

$$i_{Ls}(t_5) = I_k \tag{16}$$
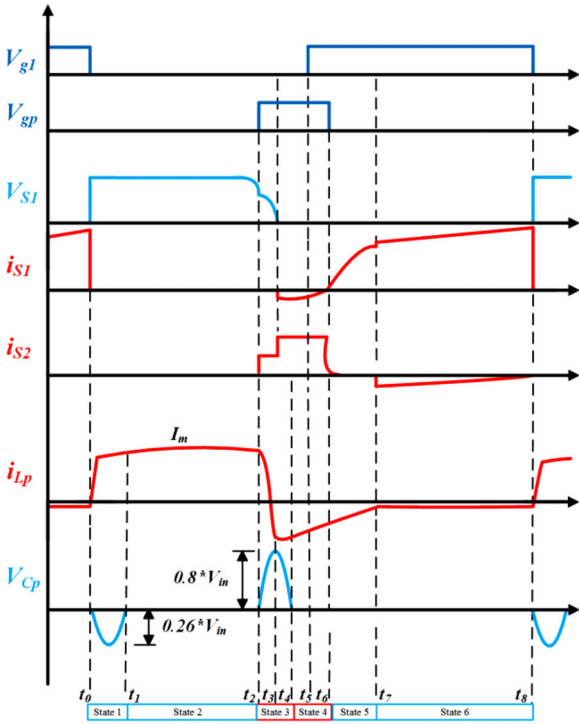
$$V_{Cs}((t) = 0. \tag{17}$$

FIGURE 6 Steady-state waveforms: buck mode (V_{g1}: gate voltage S_1; V_{gp}: gate voltage S_p; V_{S1}: collector–emitter voltage S_1; i_{S1}: current through S_1; i_{Sp}: current through S_p; i_{Lp}: resonant inductor L_p current; V_{Cp}: voltage across resonant capacitor C_p

Interval (t_6–t_7): At t_6, S_2 current starts to increase gradually the level of output current and then at t_6, it reaches to maximum output current. C_s discharges from $-V_o$ and L_s current decreases linearly. The equations for V_{Cs} and i_{Ls} are as follows:

$$i_{Ls}(t) = I_{Ls}(t_6) \cos \omega(t - t_6) \tag{18}$$

$$V_{Cs}(t) = -Z \sin \omega(t - t_6) \tag{19}$$

$$V_{Cs}(t) = \frac{-\alpha I_{in}}{V_o} \sin \omega(t - t_6). \tag{20}$$

Interval (t_7–t_8): This interval begins when the body diode of S_s starts conducting. The current through S_2 is maintained at the level of output current. Throughout this interval, energy is accumulated by L via V_1–L–S_2.

2.2 | Buck mode

This mode of operation is described with the help of steady-state waveforms as shown in Figure 6. Furthermore, all the intervals are classified into six states, states 1–6. The time intervals t_2–t_3 and t_3–t_4, t_4–t_5 and t_5–t_6 are categorised into two states: states 3 and 4, respectively. States 1 and 3 are resonant while the rest are non-resonant. The equivalent schematics of each interval with current flow directions are shown in Figures 7(a)–(d) and 8(a)–(c). When this converter is operating in
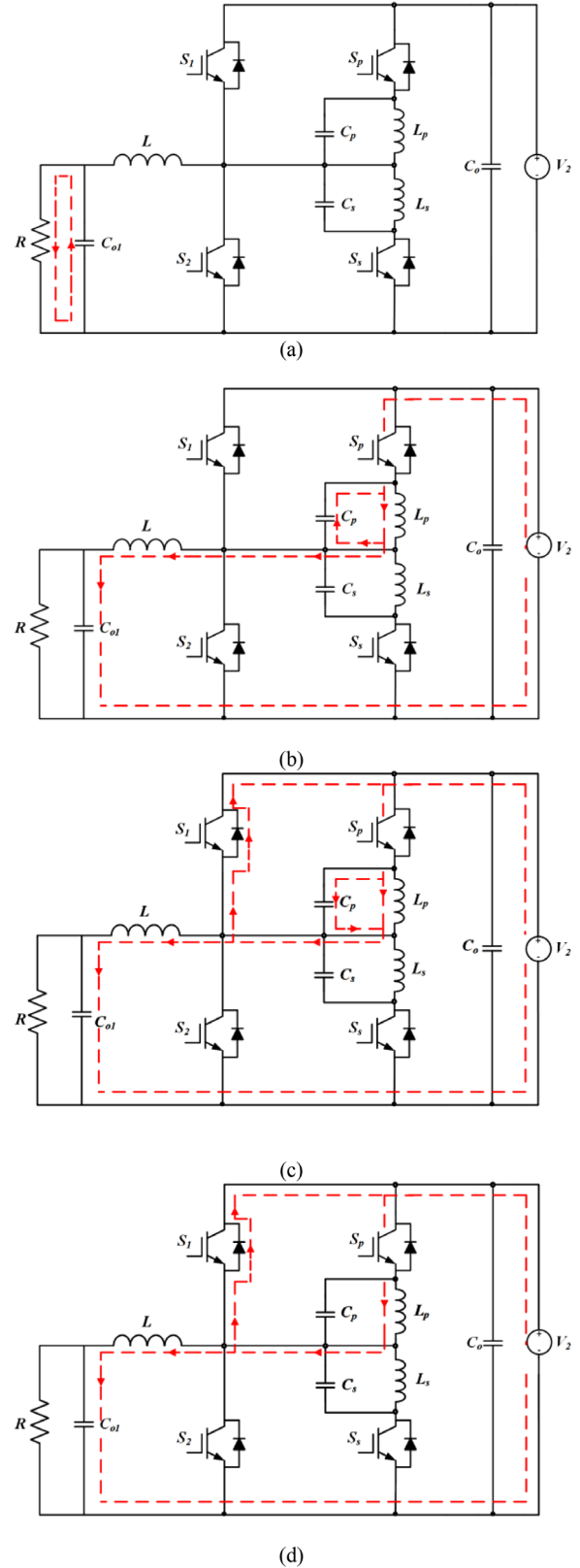

FIGURE 7 Equivalent current flow schematics : buck mode (a) interval (t_0–t_1), (b) interval (t_1–t_2), (c) interval (t_2–t_3) and (d) intervals (t_3–t_4), (t_4–t_5) and (t_5–t_6)
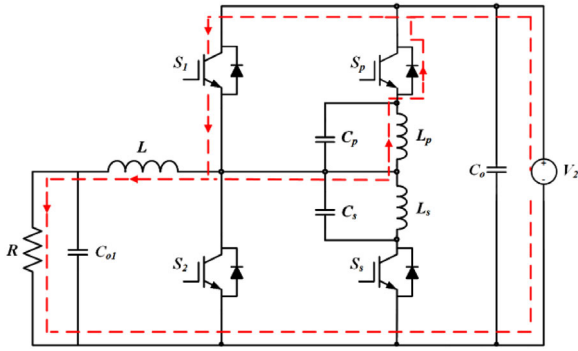
FIGURE 8 Equivalent current flow schematics : buck mode

buck mode, the IGBTs S_2, S_s are kept turned-off for the entire operation. The IGBT S_1 acts as a buck switch and the auxiliary IGBT S_p can be turned on to achieve soft-switching operation. Nevertheless, the auxiliary IGBT S_p can be turned on for a small period of time, the gate pulse V_{gp} is applied prior to that of S_1. The eight intervals of buck operations are described as below:

Interval (t_0--t_1): This stage begins when all switching devices are in turned off condition, since L_p and C_p are resonating with each other. The L_p and C_p are resonating until t_1, as the resonant capacitor C_p starts charging in the reverse direction up to $0.26 \times V_{in}$ and then discharges completely at t_1. At t_1, i_{Lp} reaches a constant value, that is, output current:

$$V_{Cp}(t) = -Z \sin \omega (t - t_0) \tag{21}$$

$$i_{Lp}(t) = i_{Lp}(t_6) \cos \omega (t - t_0) \tag{22}$$

$$V_{Cp}(t) = -\frac{\alpha I_{in}}{V_o} \sin \omega (t - t_0). \tag{23}$$

Interval (t_1–t_2): From the previous stage, all switches are in turned off condition, since there is no power delivered to the load until t_2:

$$i_{Lp} = 0 \tag{24}$$

$$V_{Cs} = 0. \tag{21}$$

Interval (t_2–t_3): This interval begins when S_p is turned on. The voltage across S_1 starts decreasing smoothly and reduces to zero at t_3. The current through L_p linearly decreases to $-I_m$. The capacitor C_p begins to charge and is fully charged at t_3, which is equal to $0.8 \times V_2$, as both L_p and C_p are resonating with each other.

$$V_{Cp}(t) = Z \sin \omega (t - t_2) \tag{25}$$

$$i_{Lp}(t) = i_{Lp}(t_2) \cos \omega (t - t_2) \tag{26}$$

$$V_{Cp}(t) = \frac{\alpha I_{in}}{V_o} \sin \omega (t - t_2) \tag{27}$$

$$I_k = i_{Ls}(t_3) \cos \omega (t_3 - t_2) \tag{28}$$

$$\Delta t_2 = \frac{1}{\omega} \cos^{-1} \left(\frac{I_k}{I_{Lp}(t_2)} \right). \tag{29}$$

Interval (t_3–t_4): At t_3, body diode of S_1 starts conducting to allow the resonant tank current since S_p is still in conduction. The current through L_p reaches I_k and at t_4, the capacitor C_p discharges completely:

$$i_{Lp}(t) = I_k \tag{30}$$

$$V_{Cp} = 0. \tag{31}$$

Interval (t_4–t_5): During this interval, the current through L_p is maintained at $+I_m$ and V_{Cp} remains zero.

Interval (t_5–t_6): When the gate pulses V_{g1} is applied to S_1, this interval begins. Since S_1 body diode is still conducting and voltage across S_1 is zero, ZVS is obtained. At t5, S_1 body diode stops conducting and current through S_p becomes zero. The i_{Lp} remains constant, which is equal to maximum output current:

$$i_{Lp}(t) = I_k \tag{32}$$

$$V_{Cp} = 0. \tag{33}$$

Interval (t_6–t_7): At t_6, S_p is turned off and S_1 starts conducting and then i_{S1} reaches the level of output current at t_7.

Interval (t_7–t_8): During this interval, the power is delivered to the load via L–S_1–R:

$$i_{Lp}(t) = I_k \tag{34}$$

$$V_{Cp} = 0. \tag{35}$$

3 | SOFT-COMMUTATION ANALYSIS BY STATE-PLANE TRAJECTORY CURVES

The soft-commutation analysis of the proposed converter is illustrated with the help of state plane trajectory curves in this section. The current and voltage waveforms of L_p, L_s, C_p and C_s are illustrated in Figure 9(a)–(c), All the states from t_0–t_8 are represented in state plane trajectory of resonant circuit, which is depicted in Figure 10 for boost mode when $\alpha > 1$. Both boost and buck modes of operation are divided into six states, state 1 from t_0 to t_1, state 2 from t1 to t_2, states 3 and 4 are through t_2–t_6, state 5 from t_6 to t_7 and t_7–t8 as state 6. It can be seen from state plane curve that states 1, 3 and 5 are resonant regions and the rest are non-resonant. However, only S_s are in conduction state during time interval t_2–t_6.

Soft commutation of the proposed converter is obtained when $\alpha > 1$. The current, i_{Ls}, and voltage, V_{Cs}, waveforms are depicted in Figure 9(a and b) when $\alpha > 1$ for boost and buck modes, respectively, and in Figure 9(c) when $\alpha < 1$, for both the modes. It can be seen from Figure 9(a) that ZVS turn-on
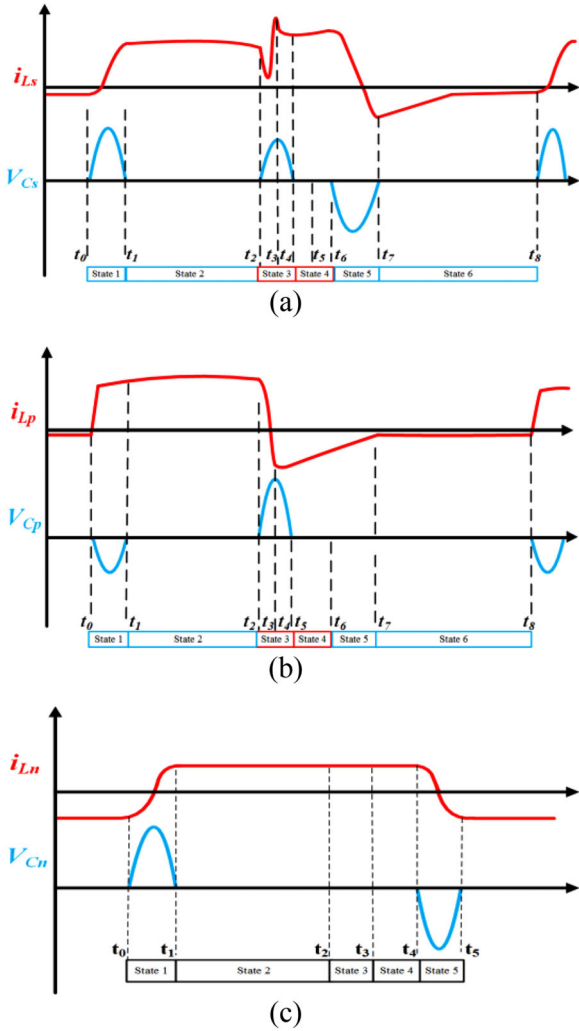
FIGURE 9 Current and voltage waveforms of resonant inductor and capacitor: boost mode (buck mode) – (a) boost mode when $\alpha > 1$, (b) buck mode when $\alpha > 1$ and (c) boost and buck modes when $\alpha < 1$
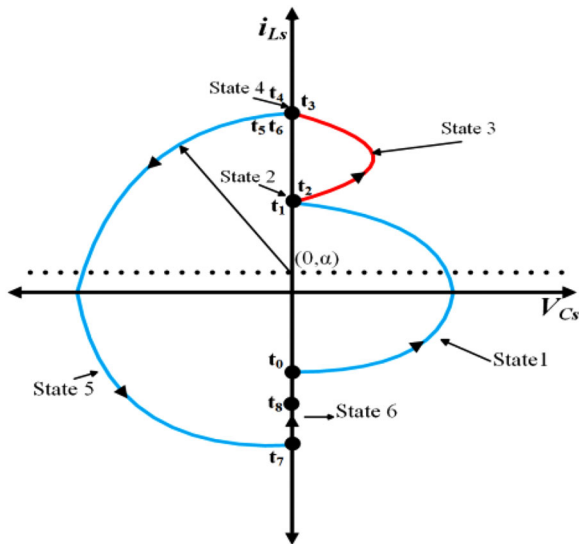

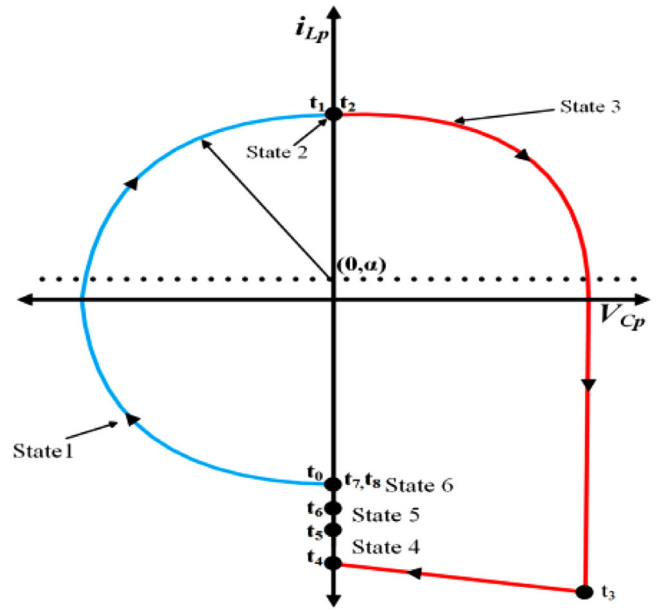**FIGURE 10** State-plane trajectory of resonant circuit: $\alpha > 1$ (boost mode)

FIGURE 11 State-plane trajectory of resonant circuit: $\alpha > 1$ (buck mode)

operation is achieved in the time intervals, t_2–t_3 and t_3–t_4. It can also be seen that the inductor L_s current linearly increases to the level of I_k and C_s charges to the input voltage level and discharges by the end of this interval.

The resultant current and voltage waveforms of L_p and C_p, when $\alpha > 1$ for buck mode operation, are depicted in Figure 9(b). It is observed from the waveform, the ZVS turn on is achieved during the time interval, t_2–t_6. The interval t_2–t_6 is classified into two states, states 3 and 4. Figure 9(c) represents the hard-switching condition with $\alpha < 1$ as there is no resonance occurring during t_2–t_4. The reliable soft-switching operation is only possible for the proposed converter is when $\alpha > 1$ and there is a guaranteed ZVS turn on operation without additional losses. Figure 10 shows state plane trajectory curve plotted for boost mode with the aid of theoretical waveforms shown in Figure 9(a). The intervals t_2–t_3, t_3–t_4, t_4–t_5 and t_5–t_6 are considered as two states, namely, states 3 and 4. These states can be recognised as soft-commutation time intervals since remaining, namely, states 1, 2, 5 and 6 are non-soft-commutation time intervals.

The state plane trajectory curves are also plotted in the Figure 11 with the help of Figure 9(b) for buck mode. The soft-commutation time intervals t_2–t_6 are similar to boost mode, except states 1 and 5. Figure 12 shows the trajectory curve plotted for both boost and buck modes when $\alpha < 1$. The current, i_n (i_{Ls} or i_{Lp}) and voltage, V_{enn} (V_{Cs} or V_{Cp}) waveforms are shown in Figure 9(c). It can be seen that states 3 and 4 in the interval t_2–t_4 are non-resonant state as soft commutation does not occur. During the interval, t_2–t_4, either in buck or boost mode, auxiliary switch S_p or S_s is turned on but current, i_{Ln} is constant and V_{Cn} is 0, as resonance does not occur between them. Similarly in the boost mode, the switch S_s is turned on, the current i_{Ls} is constant and V_{Cs} is 0. The best suitable soft-switching region that can be obtained for this converter is when $\alpha > 1$.
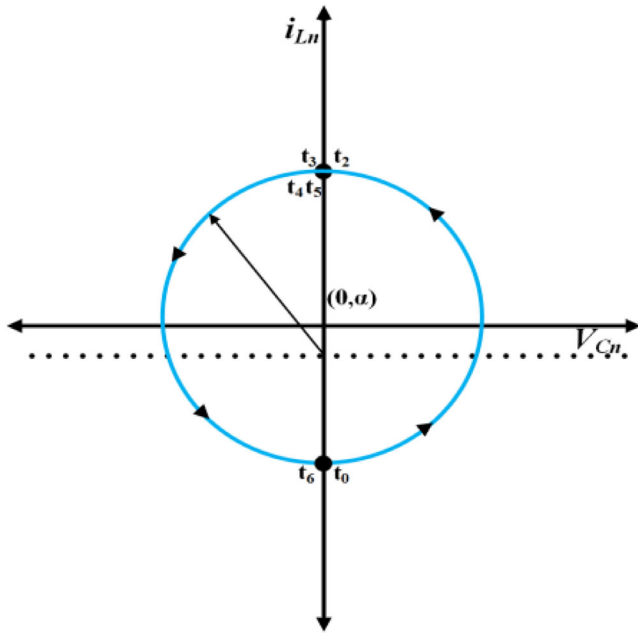
FIGURE 12 State-plane trajectory of resonant circuit: $\alpha < 1$

TABLE 1 Components and parameters

Parameters	Symbol	Value
Switching frequency	f_s	50 kHz
Main switches	$S_{1\text{-}2}$	IKW40H1203
Auxiliary switches	$S_s\text{-}S_p$	IKW40H1203
Resonant inductors	L_s, L_p	10 μH (ferrite core E-70)
Capacitor	C_s, C_p	3 nF (FKP-1)
Inductor	L	100 μH
Input voltage	V_1	175 V
Output Voltage	V_o	385 V
Output power	P_o	2 kW
Output capacitor	C_o	470 μF
Input inductor	L	100 μH

4 | DESIGN ANALYSIS

To verify the principle of operation of proposed converter, the following parameters are considered: $V_{in} = 175$; $V_{out} = 385$ V; switching frequency, $f_s = 50$ kHz; and output power, $P_o = 2$ kW.

Average input current of the converter is given by Equation (36):

$$I_{in} = I_L - I_o. \tag{36}$$

For boost and buck modes of operation, the input inductor current is calculated by Equation (37):

$$I_L = \frac{V_{in} + V_o}{V_{in} V_o} P_o \tag{37}$$

$$i_{L(max)} = 16 \text{ A}.$$

The characteristic impedance of the resonant cell is calculated as

$$Z = \sqrt{\frac{L_n}{C_n}} = 57.7\Omega. \tag{38}$$

The values of resonant inductors L_s, L_p and capacitors C_s, C_p are chosen from Equation (15):

$$L_n = L_p = L_s = 10 \text{ } \mu H;$$
$$C_n = C_p = C_s = 3 \text{ } nF.$$

The peak voltage and current rating of the switching devices and passive devices are calculated by the following equations:

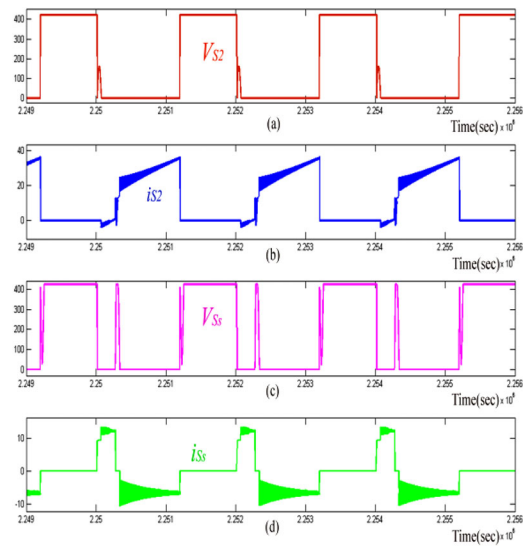$$V_{S1} = V_{Saux} = V_{in} + V_o \tag{38}$$

FIGURE 13 Simulated results: (a) V_{S2}, (b) i_{S2}, (c) V_{Ss} and (d) i_{Ss} – boost mode

$$I_{S1} = I_{S2} = I_L \tag{39}$$

$$I_{aux} = I_L + \frac{V_{in} + V_o}{Z}. \tag{40}$$

The selection of voltage and current ratings of main and auxiliary IGBTs is based on equations (38)–(40), respectively. The maximum voltage rating, 1200 V and current rating 40 A for all IGBTs are taken into consideration for experimental analysis.

5 | SIMULATION ANALYSIS

The proposed converter-designed model is simulated on MATLAB-Simulink. The parameters used for the simulation are given in Table 1. The soft-switching ZVS turn-on operation is obtained; the simulated waveforms of V_{S2}, i_{S2}, V_{Ss} and i_{Ss} are shown in Figure 13. Figure 14 shows the resonant inductor
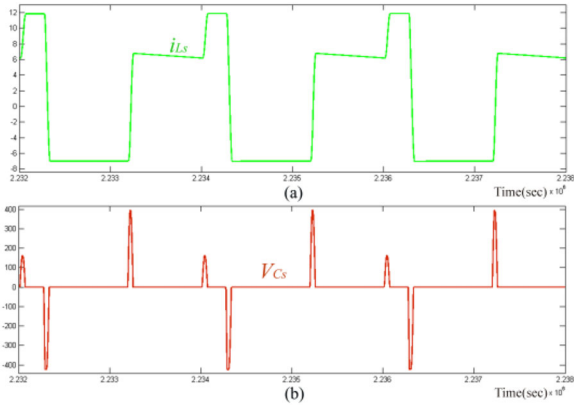
FIGURE 14 Simulated results: (a) i_{Ls} and (b) V_{Cs} – boost mode
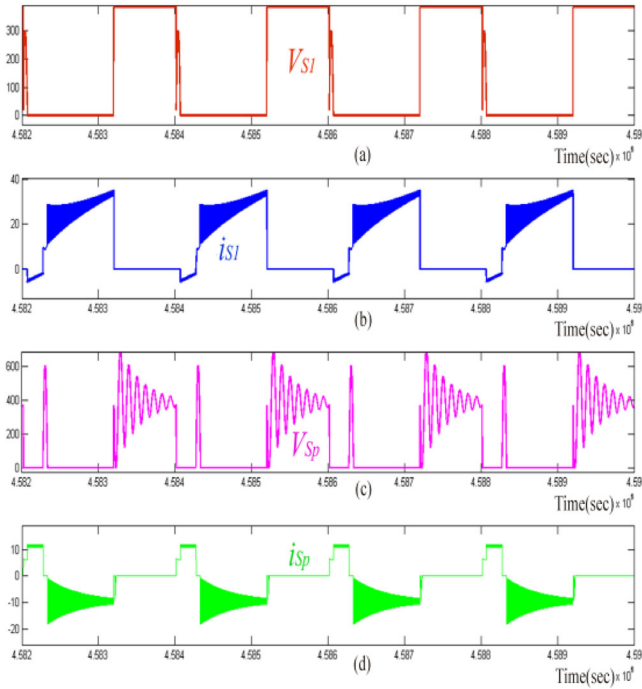

FIGURE 15 Simulated results: (a) V_{S2}, (b) i_{S2}, (c) V_{Ss} and (d) i_{Ss} – buck mode

FIGURE 16 Simulated resultsI (a) i_{Lp} and (b) V_{Cp} – buck mode

FIGURE 17 Experimental waveforms (boost mode) – V_{S2}: collector–emitter voltage of S_2 (200 V/div); i_{S2}: collector current of S_2 (10 A/div); V_{Ss}: collector–emitter voltage of S_s (100 V/div); i_{Ss}: collector current of S_s (2 A/div)

current, i_{Ls} and capacitor voltage, V_{Cs}. The simulated waveforms of V_{S1} and i_{S1}, V_{Sp} and i_{Sp}, when the converter is operated in buck mode are illustrated in Figure 15(a)–(d). Figure 16(a) and (b) represents the waveforms of inductor current and capacitor voltages for buck mode.

6 | EXPERIMENTAL ANALYSIS

In order to validate the simulation analysis, the experimental prototype is implemented on 175 V/385 V/2 kW converter system operated at 50 kHz switching frequency. The parameters given in Table 1 are used for the experimental evaluation. When this converter is operated in boost mode, the source voltage, 175 V gives an output voltage, 385 V at 5 A output current.
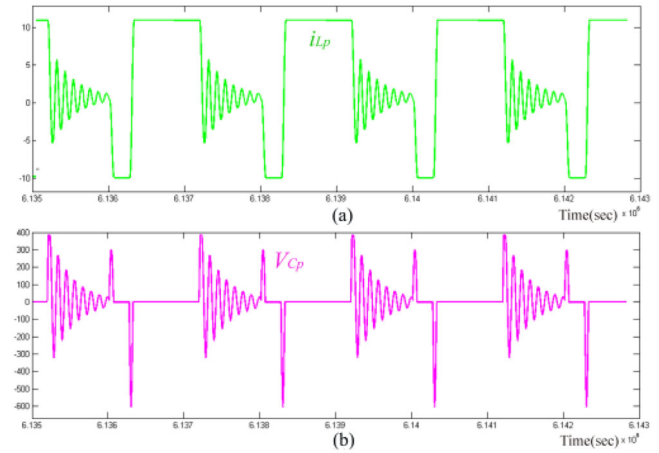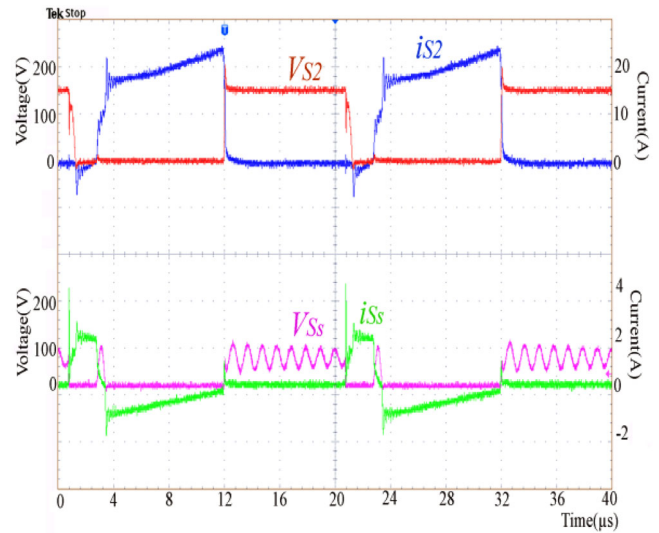
Both main IGBTs and auxiliary IGBTs are implemented with four numbers of IKW40H1203 (1200 V/40 A), and two pairs of two turn Ferrite core E-70s with an air gap of 3.5 mm used to form 10 µH resonant inductor. In order to make 3 nF resonant capacitor, parallel connection of three numbers of 1000 pF polypropylene film type (WIMA FKP-1) capacitors are used. The proposed converter is tested in boost and buck modes, separately. To validate the theoretical analysis and performance of the proposed converter, it is evaluated on 2 kW laboratory prototype. In both boost and buck modes of operations, the auxiliary switches (S_s, S_p) are operated with a constant duty cycle, 0.10. Measured voltage and current waveforms of the main switches, S_2 and S_s, when this converter is operated in boost mode, are shown in Figure 17. It can be seen that the switch, S_2 is turned-on with ZVS and the reverse current flow through the diodes of S_2 and S_s is minimal. The turn on loss of main IGBT, S_2 is reduced due to ZVS in boost mode. However, insignificant
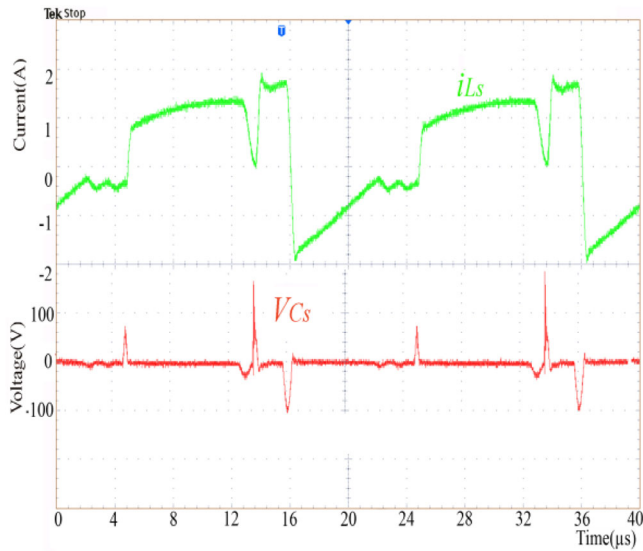
FIGURE 18   Experimental waveforms (boost mode) – i_{Ls}: current through L_s (1 A/div); V_{Cs}: voltage across C_s (100 V/div)
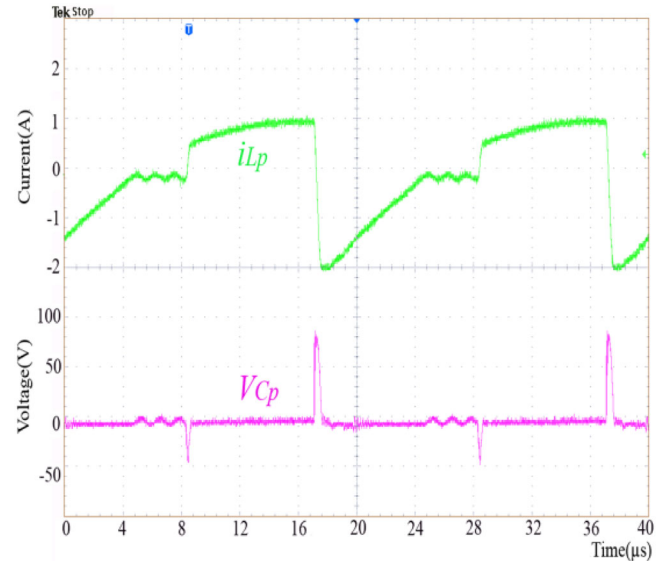

FIGURE 20   Experimental waveforms (buck mode) – i_{Lp}: current through L_p (1 A/div); V_{Cp}: voltage across C_p (50 V/div)
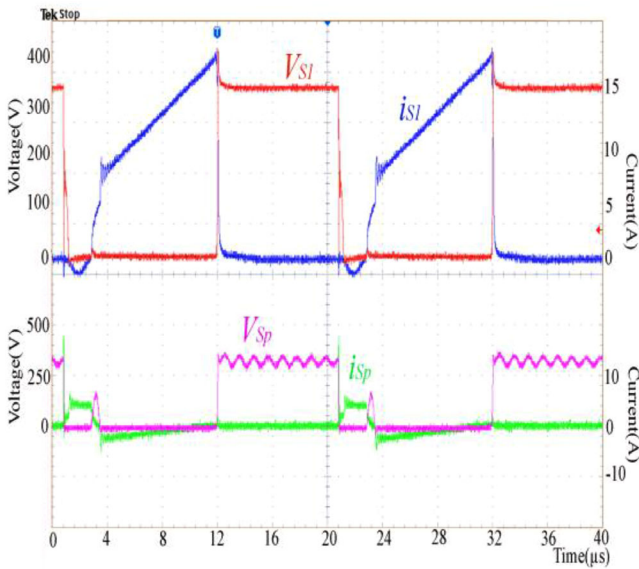

FIGURE 19   Experimental waveforms (buck mode) – V_{S1}: collector–emitter voltage of S_1 (100 V/div); i_{S1}: collector current of S_1 (5 A/div); V_{Sp}: collector–emitter voltage of S_p (250 V/div); i_{Sp}: collector current of S_p (10 A/div)

ripples appear across collector–emitter voltage V_{Ss}, which can affect neither efficiency nor voltage stress. The measured waveforms of current through auxiliary inductor, L_s (i_{Ls}) and voltage across the capacitor, C_s (V_{Cs}), when the converter is operated with 0.50 duty ratio in boost mode, are illustrated in Figure 18. It is observed from the measured waveforms that the capacitor, C_s is charging and discharging to the levels of half of the input voltage and the peak of the current in the inductor is about −1.5 to 1.5 A. Similarly, the proposed converter is also tested in buck mode with an input voltage of 385 V and operated at a maximum output power of 2 kW. Figure 19 shows the voltage and

current waveforms of the main and auxiliary IGBTs. It can be seen that the ZVS turn on is obtained for S_1 and ZCT turn-off is obtained for auxiliary IGBT, S_p. It is also observed that the auxiliary IGBT, S_p peak current is 6 A, which is equal to the input current. Figure 20 shows the voltage and current waveforms of C_p and L_p. It is observed from these results that the obtained experimental waveforms of L_p and C_p are identical with those of the theoretical analysis. It can be seen that the peak current from the waveforms of resonant inductor, L_p is about 1–1.5 A as there are no current stresses through the main IGBT, S_1 and auxiliary IGBT, S_p. When converter is operated in buck mode with two different duty ratios namely, 0.55 and 0.6, there is a clear turn on transition of ZVS on main IGBT and auxiliary IGBT which are shown in Figure 21(a) and (b), respectively. It can be seen that there is a very small amount of reverse current flowing through the diode of S_1 when this converter is operated at 0.55 and 0.60 duty cycles. The obtained experimental waveforms are same as simulation results, except for some parasitic oscillations. The efficiency of the proposed converter is measured in boost mode from the 200 W to 2 kW output power levels. The boost and buck mode efficiency curves are depicted in Figure 22. The efficiency curve is plotted for measured values when this converter is operated in boost mode with an input voltage, 175 V at 0.45 duty cycle and maximum output power of 2 kW and in buck mode with input voltage of 330 V and duty cycle, 0.60. The maximum efficiency of 96.5% is achieved at 2 kW output power with duty cycle, 0.45. The maximum efficiency obtained in boost mode is 96.5%. The proposed converter has superior performance at 0.45 duty cycle. Similarly, converter efficiencies are also measured for buck mode and the efficiency versus output power curve is shown in Figure 22. When this converter is operated in buck mode, it displayed better performance, mainly with 0.60 duty cycle. This performance analysis can be helpful to choose the optimised high efficient operating point for high-power applications.
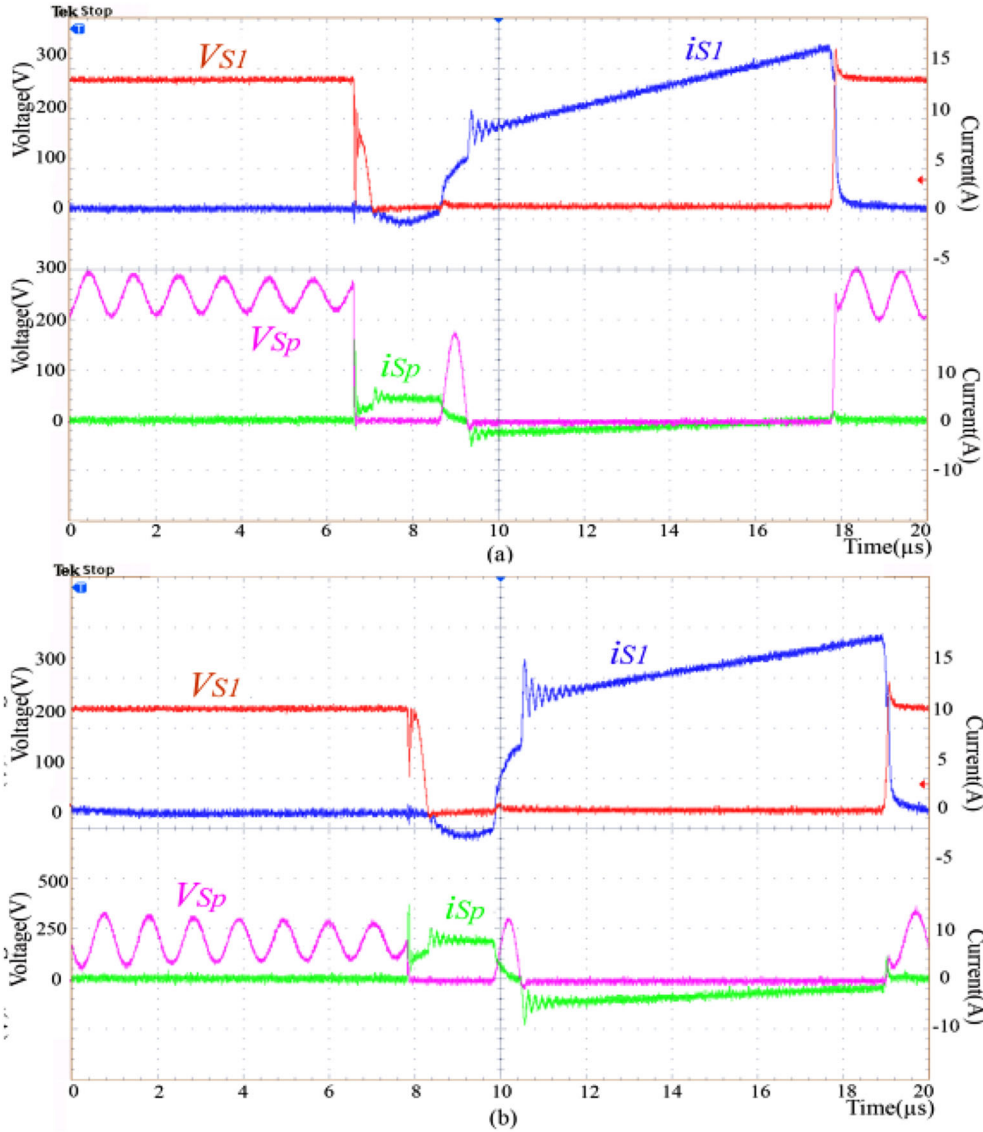
FIGURE 21 Experimental waveforms: ZVS turn-on transitions of switches S_1, S_p – (a) with duty cycle 0.55 and (b) with duty cycle 0.60
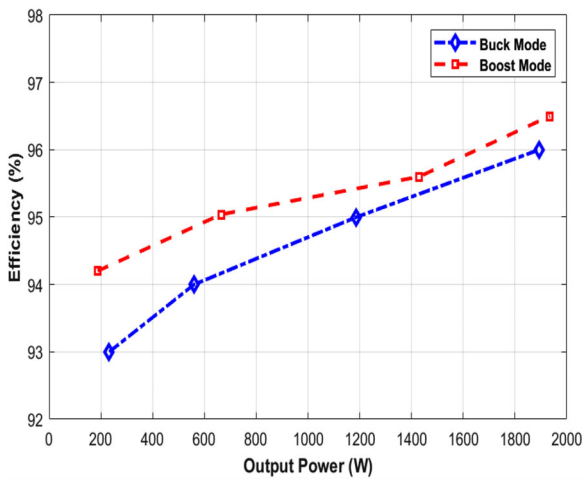

FIGURE 22 Efficiency curves of proposed converter: boost and buck modes

7 | CONCLUSION

This paper presents a new design of soft-switched non-isolated DC–DC converter for energy storage applications. The main switches are operated with ZVS turn-on and auxiliary switches are turned off with ZCS. This is realised by developing dual active series resonant networks. These two networks ensured the ZVS over the entire operating range in both boost and buck modes. Besides, the auxiliary switches are also soft-switched to prevent additional losses. A 2 kW prototype is built and tested to verify operation of this converter. A full load maximum efficiency of 96.5% in boost mode is recorded at 50 kHz operating frequency and 0.45 duty cycle. On the other hand, when the converter is operated in buck mode at 0.6 duty cycle with the same operating frequency, an efficiency of 96% is obtained. Moreover, the reverse recovery problem of the main IGBT body diodes and turn on losses are reduced as well. Hence, it can

be concluded that the proposed design provides high efficiency through soft-switching for a wider range of output power.

ORCID

Veera Venkata Subrahmanya Kumar Bhajana https://orcid.org/ 0000-0003-3830-7422
Chitti Babu B. https://orcid.org/0000-0002-3595-1223

REFERENCES

1. Rosas-Caro, J.C., et al.: A DC-DC multilevel boost converter. IET Power Electron. 3(1), 129–137 (2010)
2. Xian, L., et al.: Subproportion control of double input buck converter for fuel cell/battery hybrid power supply system. IET Power Electron. 7(8), 2141–2150 (2014)
3. Xiao, H., Xie, S.: Interleaving double-switch buck-boost converter. IET Power Electron. 5(6), 899–908 (2012)
4. Liao, H., et al.: Non-inverting buck–boost converter with interleaved technique for fuel-cell system. IET Power Electron. 5(8), 1379–1388 (2012)
5. Onar, O.C., Khaligh, A.: A novel integrated magnetic structure based DC/DC Converter for hybrid battery/ultracapacitor energy storage systems. IEEE Trans. Smart Grid 3(1), 296–307 (2012)
6. Ardi, H., et al.: Non-isolated bidirectional DC-DC converter analysis and implementation., IET Power Electron. 7(12), 3033–3044 (2014)
7. Wu, H., et al.: High step-up/step-down soft-switching bidirectional DC–DC converter with coupled-inductor and voltage matching control for energy storage systems. IEEE Trans. Ind. Electron. 63(5), 2892–2903 (2016)
8. Jiang, L., et al.: A Novel soft-switching bidirectional DC–DC converter with coupled inductors. IEEE Trans. Ind. Appl. 49(6), 2730–2740 (2013)
9. Shaneh, M., et al.: Non-isolated interleaved bidirectional DC–DC converter with high step voltage ratio and minimum number of switches. IET Power Electron. 12(6), 1510–1520 (2019)
10. Muhammad, M., et al.: A nonisolated interleaved boost converter for high-voltage gain applications. IEEE J. Emerging Sel. Top. Power Electron. 4(2), 352–362 (2016)
11. Pan, T., et al.: Topology optimisation and current sharing strategy of interleaved bidirectional DC/DC converter with coupling technique. IET Power Electron. 11(15), 2470–2480 (2018)
12. Chen, G., et al.: A family of zero-voltage-switching magnetic coupling nonisolated bidirectional DC–DC converters. IEEE Trans. Ind. Electron. 64(8), 6223–6233 (2017)
13. Zhang, Y., et al.: A soft-switching bidirectional DC–DC converter for the battery super-capacitor hybrid energy storage system. IEEE Trans. Ind. Electron. 65(10), 7856–7865 (2018)
14. Ardi, H., et al.: Analysis and implementation of a nonisolated bidirectional DC–DC converter with high voltage gain. IEEE Trans. Ind. Electron. 63(8), 4878–4888 (2016)
15. Das, P., et al.: A nonisolated bidirectional ZVS-PWM active clamped DC–DC converter. IEEE Trans. Power Electron. 24(2), 553–558 (2009)
16. Mousavinezhad Fardahar, S., Sabahi, M.: High step-down/high step-up interleaved bidirectional DC–DC converter with low voltage stress on switches. IET Power Electron. 13(1), 104–115 (2020)
17. Zhang, Y., et al.: Analysis and research of a soft-switching bidirectional DC–DC converter without auxiliary switches. IEEE Trans. Ind. Electron. 65(2), 1196–1204 (2018)
18. Yang, J., Do, H.: High-efficiency bidirectional DC–DC converter with low circulating current and ZVS characteristic throughout a full range of loads. IEEE Trans. Ind. Electron. 61(7), 3248–3256 (2014)
19. Ashique, R.H., Salam, Z.: A high-gain, high-efficiency nonisolated bidirectional DC–DC converter with sustained ZVS operation. IEEE Trans. Ind. Electron. 65(10), 7829–7840 (2018)
20. Mohammadi, M.R., Farzanehfard, H.: A new family of zero-voltage-transition nonisolated bidirectional converters with simple auxiliary circuit. IEEE Trans. Ind. Electron. 63(3), 1519–1527 (2016)